Drug Design, Development and Therapy

Dovepress
Taylor & Francis Group

Open Access Full Text Article

ORIGINAL RESEARCH

FoxO1 as a Hub in Immunosenescence Induced by Hepatocellular Carcinoma and the Effect of Yangyin Fuzheng Jiedu Prescription

Yuqing Xie[1,2,*], Fengna Yan[1,2,*], Xiaoli Liu[1,2], Lihua Yu[1,2], Huiwen Yan[1,2], Zimeng Shang[1,2], Yaxian Kong[3], Zhiyun Yang[1,2]

[1]Center of Integrative Medicine, Beijing Ditan Hospital, Capital Medical University, Beijing, People's Republic of China; [2]Capital Medical University Research and Translational Laboratory for Traditional Chinese Medicine in the Prevention and Treatment of Infectious Severe Hepatitis, Beijing, People's Republic of China; [3]Beijing Key Laboratory of Emerging Infectious Diseases, Institute of Infectious Diseases, Beijing Ditan Hospital, Capital Medical University, Beijing, People's Republic of China

*These authors contributed equally to this work

Correspondence: Zhiyun Yang, Center of Integrative Medicine, Beijing Ditan Hospital, Capital Medical University, Beijing, People's Republic of China, Email yangzhiyun2016@163.com; Yaxian Kong, Beijing Key Laboratory of Emerging Infectious Diseases, Institute of Infectious Diseases, Beijing Ditan Hospital, Capital Medical University, Beijing, People's Republic of China, Email kongyaxian@ccmu.edu.cn

Purpose: Yangyin Fuzheng Jiedu Prescription (YFJP) is a traditional Chinese medicine (TCM) used for the treatment of hepatocellular carcinoma (HCC). However, the potential mechanisms remain unclear. The objective of this study is to clarify the mechanism of action of YFJP in treating HCC.

Methods: By constructing networks, the active components and molecular targets of YFJP in the treatment of HCC were explored. The TCGA database was utilized to analyze the correlation between the core target and the overall survival (OS) of patients with HCC. The regulatory effect of YFJP on T cell was evaluated by detecting samples from patients with HCC. The molecular mechanism of YFJP in treating HCC was validated through in vivo and in vitro experiments.

Results: Constructing networks and analyse indicated that the key targets of YFJP in the treatment of HCC is FoxO1. Analysis of the HCC patient cohort in the TCGA database demonstrated that FoxO1 is an independent protective factor for overall survival in patients with HCC. Pathway enrichment analysis enriched FoxO signaling pathway and Cellular senescence pathway. Prospectively collecting samples from patients with HCC suggested that YFJP treatment increased the proportion of $CD8^+$ T cells. In vivo experiments showed that YFJP treatment ameliorated $CD8^+$ T cell senescence in tumor-bearing mice. Western blot, flow cytometry and multi-color immunofluorescence co-staining showed that YFJP treatment increased the expression of FoxO1 in $CD8^+$ T cells. The primary $CD8^+$ T cells were sorted and co-cultured with an HCC cell line in vitro. Inhibiting the expression of FoxO1 in $CD8^+$T cells confirmed that FoxO1 is a key target for YFJP to improve the senescence of $CD8^+$ T cell.

Conclusion: FoxO1 is the key molecular target of YFJP in improving $CD8^+$ T cell senescence in HCC. This study preliminarily clarified the mechanism of YFJP in regulating immunosenescence of HCC.

Keywords: hepatocellular carcinoma, senescence, T cell, network pharmacology, Yangyin Fuzheng Jiedu Prescription

Introduction

Primary liver cancer (PLC) is a critical worldwide health issue, with almost one million new cases reported in 2023, hepatocellular carcinoma (HCC) constitutes the predominant variant of PLC, representing 90% of all occurrences.[1] The onset of HCC is insidious and diagnosis often occurs at an advanced stage. According to several clinical trials, few patients with HCC obtain durable clinical benefits from systemic treatments, ICI therapy is associated with a variety of immune-related adverse reactions.[2] HCC remains a significant public health challenge with a poor prognosis. The five-year survival rate of HCC is only 20%, and the median survival time is only 1–2 years for patients with advanced HCC.[3]

Received: 25 September 2024
Accepted: 10 February 2025
Published: 5 March 2025

Graphical Abstract

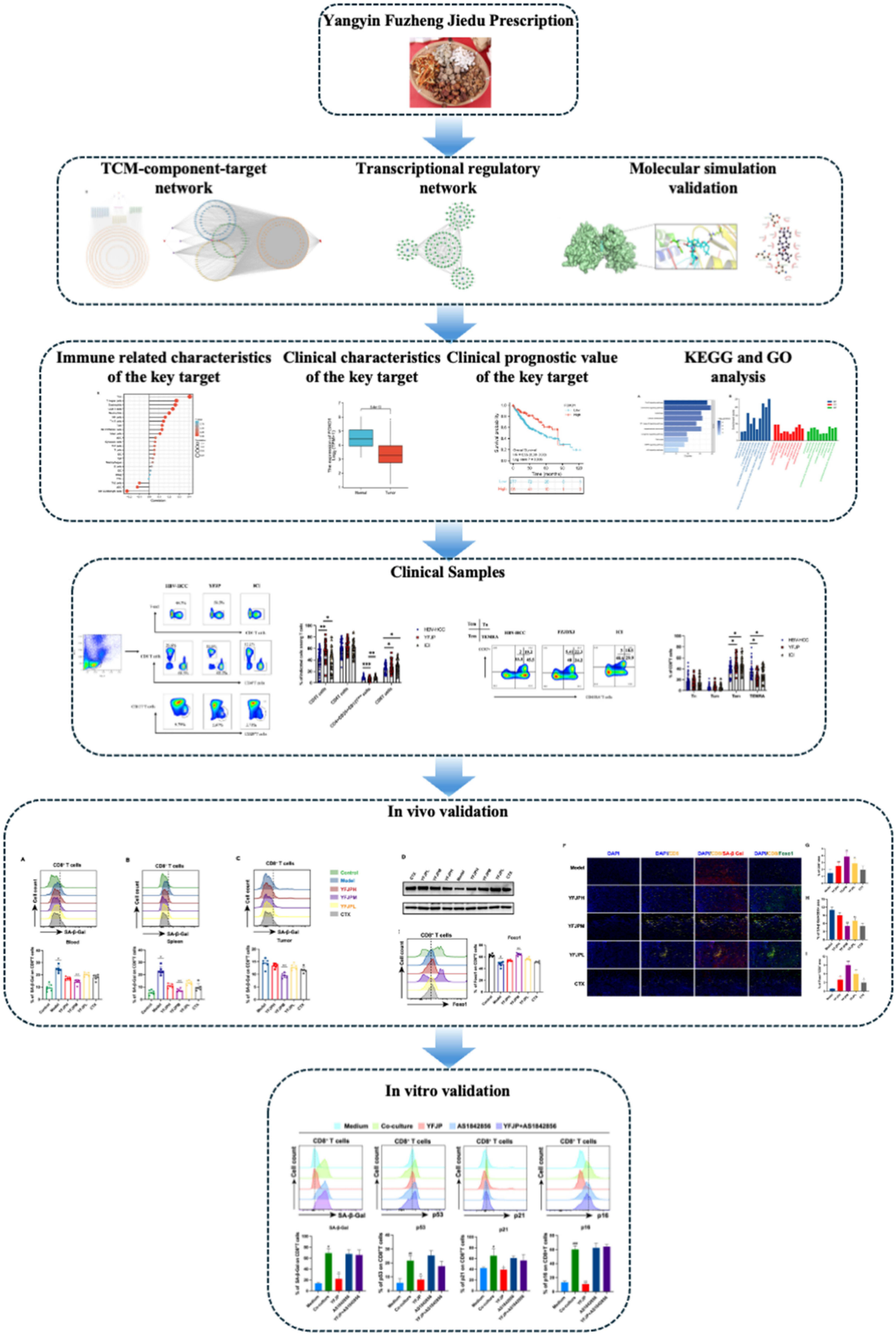

Traditional Chinese Medicine (TCM) has a long-standing history of being used in the treatment of HCC. Yangyin Fuzheng Jiedu Prescription (YFJP) has been employed in the treatment of HCC for more than a decade,[4] with obvious clinical efficacy and good safety,[5] and has been granted multiple national patents (patent no.:ZL202110889980.5), (patent no.: ZL202110500342.X). YFJP consists of *Glehnia littoralis* (A. Gray) F. Schmidt ex Miq. (Chinese name: BeiShashen), *Ophiopogon japonicus* (Thunb). Ker Gawl. (Chinese name:MaiDong), *Astragalus mongholicus* Bunge. (Chinese name: Huangqi), *Atractylodes macrocephala* Koidz. (Chinese name: Baizhu), *Bupleurum chinense* DC. (Chinese name: Chaihu), *Sophora flavescens* Aiton (Chinese name: Kushen), *Vincetoxicum mukdenense* Kitag. (Chinese name: Xuchangqing), and *Scleromitrion diffusum* (Willd). R.J.Wang (Chinese name: Baihua Sheshe Cao) (Table 1). Based on our previous large-sample retrospective cohort study, YFJP can improve the 5-year cumulative survival rate of patients with HCC and prolong the median survival time via a dose-effect relationship.[5] YFJP was also found to mediate the action of several HCC-related genes.[6] Preliminary screening was performed to explore the effective herbal combinations in the prescription.[7] However, the molecular mechanisms underlying the therapeutic effects of YFJP require further clarification.

The development of HCC is primarily due to immune escape of tumor cells, which manifests as immune surveillance and clearance dysfunction.[8] The tumor microenvironment (TME) is a crucial site for facilitating tumor immune escape and a significant impediment to effective immunotherapy.[9] As the core of the adaptive immune system, T cells exert a key role in anti-tumor immunity. Recent investigations have demonstrated that T cell senescence significantly impacts the anti-tumor immune response.[10] The concept of immunosenescence was first proposed by Walford (1964).[11] Immunosenescence is characterized by a decline in adaptive immunity, which leads to a decline in immune function, ultimately affecting all aspects of the immune function network and promote the onset and progression of tumors.[12] Senescent cells are marked by an increase in both the mass and the number of lysosomes, linked to an increase in Senescence-associated β-galactosidase (SA-β-Gal) activity.[13] It should be noted that senescent T cells have the unique characteristics of unbalanced proportion of subsets, abnormal metabolic function, and reduced effector function. In addition, senescent T cells can secrete a large number of inflammatory cytokines, chemokines, and other immune regulatory factors. This senescence-associated secretory phenotype (SASP) can aggravate the chronic inflammatory microenvironment and promote immune escape in HCC.[14] Therefore, anti-tumor immunotherapy targeting senescent T cells is receiving increasing attention in recent years.

In the present research, network construction and molecular docking were performed to identify the active ingredients and therapeutic targets of YFJP for HCC treatment. The molecular mechanism was explored through the detection and analysis of patient samples, as well as through in vivo and in vitro experiments.

Materials and Methods

Dataset Construction

The potential components of each herb in YFJP were obtained from the TCMSP database (tcmsp-e.com).[15] Oral bioavailability (OB) greater than 30% and drug-like properties (DL) greater than 0.18 were employed to screen the potential bioactive ingredients of the eight herbal medicines. A total of 32 *Astragalus mongholicus* Bunge. ingredients,

Table 1 The Chinese Name, Latin Name, English Name and the Weight of Chinese Medical Herbs Used in YFJP

Chinese Name	Latin Name	English Name	Amount in Application (g)
Beishashen	*Glehnia littoralis* (A. Gray) F. Schmidt ex Miq.	Coastal Glehnia Root	15
MaiMendong	*Ophiopogon japonicus* (Thunb.) Ker Gawl.	Radix Ophiopogonis	15
Huangqi	*Astragalus mongholicus* Bunge.	Astragalus mongholicus	20
Baizhu	*Atractylodes macrocephala* Koidz.	Largehead Atractylodes Rh	9
Chaihu	*Bupleurum chinense* DC.	Chinese Thorowax Root	9
Kushen	*Sophora flavescens* Aiton	Lightyellow Sophora Root	9
Xuchangqing	*Vincetoxicum mukdenense* Kitag.	Paniculate Swallowworf Root	12
Baihua Sheshecao	*Scleromitrion diffusum* (Willd.) R.J.Wang	Spreading Hedyotis Herb	20

https://doi.org/10.2147/DDDT.S492576

14 *Atractylodes macrocephala* Koidz. ingredients, 56 *Bupleurum chinense* DC. ingredients, 45 *Sophora flavescens* Aiton ingredients, 6 *Vincetoxicum mukdenense* Kitag. ingredients, 7 *Scleromitrion diffusum* (Willd). R.J.Wang ingredients, 18 *Glehnia littoralis* (A. Gray) F. Schmidt ex Miq. ingredients, and 22 *Ophiopogon japonicus* (Thunb). Ker Gawl. ingredients were collected. The Mol2 profiles of each active ingredient were obtained from the PubChem database (PubChem (nih.gov)). The SwissTargetPrediction database (http://swisstargetprediction. ch/) was used to predict potential targets of each biologically active ingredient. The database was developed based on the similarity principle of chemical ligands.[16] Finally, 2,800 *Astragalus mongholicus* Bunge. targets, 1,259 *Atractylodes macrocephala* Koidz. targets, 4,957 *Bupleurum chinense* DC. targets, 4,400 *Sophora flavescens* Aiton targets, 600 *Vincetoxicum mukdenense* Kitag. targets, 700 *Scleromitrion diffusum* (Willd). R.J.Wang targets, 1,660 *Glehnia littoralis* (A. Gray) F. Schmidt ex Miq. targets, and 2,200 *Ophiopogon japonicus* (Thunb). Ker Gawl. targets were obtained. HCC-related targets were collected from the following databases: Disgenet database (DisGeNET – a database of gene-disease associations), 5,725 targets; TTD database (TTD: Therapeutic Target Database (idrblab.net)), 42 targets; Drugbank database (DrugBank Online | Database for Drug and Drug Target Info), 35 targets; GAD database (https://geneticassociationdb.nih.gov/), 41 targets; oncoDB. HCC database (http://oncodb.hcc.ibms.sinica.edu.tw/index.htm), 377 targets; and Liverome database (http://liverome.kobic.re.kr/index.php), 241 targets. Finally, 5,285 hCC-related targets were used for further analysis.

Network Construction and Analysis

Cytoscape software 3.9.1 was used for network construction. In this study, the TCM-component–target-disease, protein-protein interaction (PPI), and transcriptional regulation networks were constructed. PPIs were collected from the STRING database (STRING: functional protein association networks (string-db.org)).[17] Topological and cluster analyses were performed to screen core subnetworks. The topological analysis was performed using the Cytoscape plugin network analyzer. Cluster analysis was performed based on MCODE and ClusterONE to explore the closely connected core subnetworks that play important functions in the network.

Molecular Docking

The protein crystal structures were downloaded from the PDB database (RCSB PDB: Homepage) (Methot < 2). After the crystal structure was imported into Autodock tools 4.1.2, the water molecule and hydrogen atom in the protein were deleted, and the charge was added. MGL Tools 1.5.7 was then used to define the active site in the protein. The 3D structures of the key components were obtained from the PubChem database (PubChem (nih.gov)). The ligand files were converted to pdb format using Open Babel 2.4.1, and then the ligands were preprocessed using the Autodock Tools software. Finally, semi-flexible docking of the protein and ligand was performed using Autodock Vina 1.1.2 to obtain the binding energy between the key targets and key components, which can reflect the binding activity of the protein and ligand. Finally, Pymol 2.5.8 was used for 3D visualization of the protein-ligand complex while LIGPLOT 2.2 was used for 2D visualization of the protein-ligand complex.

Construction of Transcriptional Regulatory Network and Bioinformatics Analysis

The promoter sequences from the first 2000 nt to the last 100 nt of the core gene exons were obtained from the UCSC database (UCSC Genome Browser Home)[18] and entered into the PROMO database to predict the transcription factors regulated by the key targets.

The mRNA expression levels and clinical information of 407 hCC samples and 58 adjacent tissue samples were obtained from TCGA database (https://portal.gdc.cancer.gov/). The survival time, death status were obtained. Data sorting and transformation were performed using R software. The levels of FOXO1 expression in separate HCC tissues and its correlation with clinicopathological features were investigated.

Patient samples were categorized into two distinct cohorts: one with high FOXO1 mRNA expression and the other with low expression, stratified by the median value of FOXO1 mRNA levels. We conducted an analysis to elucidate the correlation between FOXO1 expression levels and the clinical prognosis of patients with HCC. Subsequently, Kaplan-Meier survival curves were generated to illustrate overall survival (OS) outcomes. Based on an external cohort from the TCGA database, in conjunction with the relationship between immune cells and the HCC microenvironment, we utilized

Gene Set Enrichment Analysis (GSEA) to assess the expression differences of 24 types of tumor-infiltrating lymphocytes (TILs) in the HCC tumor microenvironment (TME) and the correlation between TILs and FOXO1 expression levels. Spearman correlation was also used to investigate their relationship.

KEGG and GO Analysis

Kyoto Encyclopedia of Genes and Genomes (KEGG) pathway enrichment as well as Gene Ontology (GO) biological function analyses were carried out using the Cytoscape ClueGO plugin. KEGG signaling pathways, biological processes (BPs), cellular components (CCs), molecular functions (MFs) were screened according to $p < 0.05$.

Human Samples

A total of 115 patients with HCC were prospectively enrolled in this research between August 2021 and June 2023 at Beijing Ditan Hospital, Capital Medical University. This research process complies with the Declaration of Helsinki and Tokyo for humans, has been approved by the Ethics Committee of Ditan Hospital, affiliated with Capital Medical University, Beijing. The first ethical review was passed on August 11, 2021 (Jing Di Lun Ke Zi 2019 No[009]-03), and the annual re-approval was conducted on July 27, 2022 (NO.DTEC-KY2023-014-02). This research has obtained informed consent from the participants. HCC was diagnosed as performed in our previous study.[19] The research did not include individuals who had HCV or HIV infections, liver diseases of non-specified etiologies, or those diagnosed with metastatic liver cancer or additional malignancies. Patients with HCC were administered with conventional therapy (n=56), YFJP (n=27), or YFJP plus ICI (n=32). Among which conventional therapy including basic treatment, antiviral therapy, surgical resection, transcatheter arterial chemoembolization, and ablative therapy. A total volume of 5 mL of peripheral blood was prospectively collected from each patient enrolled in the study. Subsequently, peripheral blood mononuclear cells (PBMCs) were isolated from the collected samples using standard protocols. The demographic characteristics of the patients can be found in Supplementary Table 1.

Preparation of YFJP

YFJP consists of 15g *Glehnia littoralis* (A. Gray) F. Schmidt ex Miq., 15g *Ophiopogon japonicus* (Thunb). Ker Gawl., 20g *Astragalus mongholicus* Bunge., 9g *Atractylodes macrocephala* Koidz., 9g *Bupleurum chinense* DC., 9g *Sophora flavescens* Aiton, 12g *Vincetoxicum mukdenense* Kitag., and 20g *Scleromitrion diffusum* (Willd). R.J.Wang. All traditional Chinese medicinal herbs were purchased from Beijing Ditan Hospital affiliated to Capital Medical University, and the quality of the purchased YFJP was confirmed by the pharmacy department. The voucher specimens of YFJP (No. DTYY20230301) was deposited in Beijing Key Laboratory of Emerging Infectious Diseases, Institute of Infectious Diseases, Beijing Ditan Hospital, Capital Medical University. The component identification of YFJP is based on the HPLC (High-Performance Liquid Chromatography) method, the conditions and detection of which has been described before.[6] The preparation method for YFJP is standardized, which is as follows: the herbs are soaked in 450 mL of ultrapure water for 20 minutes and then boiled for 40 minutes. The liquid is filtered out. Another 300 mL of ultrapure water is added and the herbs are boiled for an additional 30 minutes, after which the liquid is filtered out. Finally, the filtrates from both decoctions are mixed.

Mice and Treatment

Male BALB/c mice, aged 8 weeks were housed in a specific pathogen-free (SPF) environment throughout the study (qualification number of the mice in this batch: SCXK-Beijing-2019-0010). The experimental mice were randomly assigned into six distinct experimental groups, including Control group, Model group, YFJP high dose group(YFJPH), YFJP medium dose group(YFJPM), YFJP low dose group(YFJPL), and cyclophosphamide group(CTX), with 6 mice in each group. Excluding the Control group, mice in the remaining experimental groups were subcutaneously injected with H22 tumor cells (2×10^6 cells/mL) in the right axillary region. The Control and Model groups were treated with normal saline, and the CTX group was treated with cyclophosphamide (2mg/kg body weight). The other three groups were treated with different doses of YFJP: YFJPH (32.7 g/kg body weight), YFJPM (16.4 g/kg body weight) and YFJPL (8.2g/kg body weight) for 7 days. All treatments were performed once daily for 7 days. After treatment, anesthesia was

performed with 1.5mL intraperitoneal injection of 5% chloral hydrate (Solarbio, T8590), and then peripheral blood, tumor tissues, as well as spleens were collected.

Isolation of Lymphocytes

Peripheral blood was collected aseptically from the retroorbital venous plexus of mice. Subsequently, PBMCs were isolated by density-gradient centrifugation employing Ficoll-Paque solution. The spleens of anesthetized mice were removed, ground and filtered in a 70μm strainer and centrifuged at 300g for 5min. Spleen lymphocyte suspensions were obtained after red blood cells were lysed. Following the resection of tumor tissues, the tissues were dissected into smaller pieces and enzymatically digested using the manufacturer-recommended tumor dissociation kit (Miltenyi Biotec, catalog number 130–096-730). After filtering through a 70-μm strainer, the tumor-infiltrating lymphocytes (TILs) were isolated by centrifugation on a 30% to 70% Percoll gradient.

Western Blotting Analysis

Thirty milligrams of tumor tissue were weighed, minced, and lysed with a 250 mg/mL lysis buffer (Biyuntian Biotechnology, P0013B) at room temperature for 30 minutes. Protein concentrations were quantified with a bicinchoninic acid (BCA) protein assay kit (Biyuntian Biotechnology, P0012). Thereafter, proteins were separated according to their molecular weight via 10% SDS gel electrophoresis, transferred onto a nitrocellulose membrane via electroporation, blocked with 5% skim milk powder in Tris buffer for 2 h, and incubated with rabbit anti-mouse FoxO1 protein (diluted 1:800) (Cell Signaling Technology, #2880) at 4 °C overnight. The membranes were washed for 15 min, incubated with the secondary antibody for 2 h, and exposed to a chemiluminescence (ECL) reagent (Proteintech Group, Chicago, IL, USA). The band intensities were quantified using ImageJ_v1.8.0 software (National Institutes of Health).

Immunofluorescence and Quantitative Analysis

To detect the senescence of $CD8^+$ T cells, as well as the level of FoxO1 in the immune microenvironment of HCC, we performed multiple immunofluorescence staining using amplification (TSA) technology. The tumor tissues were dehydrated, cleared, and wax-soaked in a gradient of ethanol, xylene, and paraffin before embedding. Four-micrometer-thick sections were created for the staining process. Following the baking of the slices at 60°C for a duration of 30min, the tissue sections were dehydrated and hydrated using xylene and gradient ethanol. After antigen repair with sodium citrate, the slices were treated with 100 μL of 3% H_2O_2 for 10 min at ambient temperature, subsequently being blocked with 5% goat serum. Subsequently, the slices were treated with the primary antibody at ambient conditions for 60 min, then incubated with the secondary antibody for 15 min, and finally subjected to the tyramide signal amplification (TSA) for 10 min. These steps were repeated until completion of target antibody staining. Finally, the slices were treated with DAPI working solution at ambient temperature for a period of 10 min prior to being sealed. The primary antibodies were CD8 (Abcam, 217344), SA-β-Gal (Abcam, 203749), and FoxO1 (CST, 2880). DAPI emits blue light, FoxO1 emits green light, $CD8^+$ T cells emit yellow light, and SA-β-Gal emit red light.

Preparation of YFJP-Contained Serum

For YFJP-containing serum preparation, SPF-grade Sprague-Dawley (SD) rats weighing 180g-200g were used. All experimental animals used in our research were purchased from Beijing Sibeifu Biotechnology Co., LTD., experimental unit license number: SYXK (Beijing) 2023–0033.

SD rats were assigned into Control serum group and YFJP-containing serum group. Rats in YFJP-containing serum group were orally administrated with YFJP water decoction, rats in Control serum group were treated with equal volume of normal saline. Rats in both groups were intervened every 12h for 7 days. After the last intervention, rats were anesthetized intraperitoneally with pentobarbital (Merck, P3761), and peripheral blood samples were acquired aseptically through the abdominal aorta. Serums were collected through centrifugation at 1000g for 15min. After incubation at 56°C for 30 minutes to achieve thermal inactivation, the serums were subjected to filtration through a 0.22-micron pore filter and then stored in a −80°C freezer for future use.

Construction of Cell Co-Culture System and in vitro Blocking Experiments

After isolating spleen lymphocytes from healthy BALB/c mice, MACS MicroBeads were utilized to sort $CD8^+$ T cells following the manufacturer's guidelines (Miltenyi Biotec, 130–104-075). $CD8^+$ T cells pre-stimulated with anti-CD3 (eBioscience, 16–0031-82) (2.5 ug/mL) and anti-CD28 (eBioscience, 16–0281-86) (2.5 ug/mL) before co-culturing with H22 cell line in 96-well plates. The cell co-culture system was intervented with control serum or YFJP-contained serum. AS1842856 (MCE HY-100596) is an inhibitor of FoxO1. For the inhibiting experiment, AS1842856 (5uM) was used to pretreat the sorted $CD8^+$ T cells for 12 h before co-culturing with H22 cell line. After 24 hours, utilizing flow cytometry, the phenotypes and fuctions of $CD8^+$ T cells in the cell co-culture system were evaluated.

Flow Cytometry

Single-cell suspensions were prepared and incubated with the fluorescence-conjugated antibodies. The PBMC of patients with HCC was incubated with the following antibodies: BV786-CD3, APC-Fire750-CD4, BV510-CD8, PE-CF594-CD25, PE-CD127, AF700-CD45RA, and BV421-CCR7.

For the mouse samples, the antibodies utilized for surface antigen staining encompasses: BV786-CD3, BV510-CD4, and BUV395-CD8. The prepared single-cell suspensions were incubated with surface antibodies for 30 min before SA-β-Gal staining or intracellular staining. The staining procedure for SA-β-Gal was executed in accordance with the protocols provided by the manufacturer (Cellular Senescence Detection Kit - SPiDER-βGal, DOJINDO, SG03). After fixation and membrane disruption, intracellular staining was performed, antibodies including APC-p53, APC-p16, PE-p21, and APC-cy7-FoxO1. Cells were analyzed using the BD LSRFortessa™ Cell Analyzer (BD Biosciences) and FlowJo (Tree Star Inc).

Statistical Analysis

Continuous variables are represented as mean ± SD. The Shapiro–Wilk test was utilized to evaluate the data for normality. One-way analysis of variance (ANOVA) was used for comparison between groups with more than 2 independent samples. Tukey's multiple comparison test was used for pairwise comparisons. The disparities in the mean values of data exhibiting a normal distribution were analyzed using one-way ANOVA through the Social Science Statistical Package software (version 21.0). Spearman's rank correlation was assessed using R (v3.6.1) to examine the relationship between FoxO1 expression and TIL, as measured in TCGA. P values <0.05 were considered to indicate statistical significance.

Results and Analysis

Construction of the TCM-Component-Target Network of YFJP

The recipe of YFJP is based on traditional Chinese medicine theory. Specifically, *Astragalus mongholicus* Bunge., *Atractylodes macrocephala* Koidz. and *Bupleurum chinense* DC. strengthen the spleen, soothes the liver, and regulates qi; *Sophora flavescens* Aiton, *Scleromitrion diffusum* (Willd). R.J.Wang, and *Vincetoxicum mukdenense* Kitag. play a detoxification role; *Glehnia littoralis* (A. Gray) F. Schmidt ex Miq. and *Ophiopogon japonicus* (Thunb). Ker Gawl. have the function of nourishing Yin (Chinese Pharmacopoeia Commission, 2020). Therefore, according to the above three therapeutic effects, we divided YFJP into three groups of herbs, named Fuzheng Prescription (FZP), Jiedu Prescription (JDP), and Yangyin Prescription (YYP). The active ingredients of the three groups of disassembled prescriptions were obtained, a total of 91 FZP components, 41 YYP components, and 57 JDP components were acquired from the TCMSP database. And the therapeutic targets of the three groups of disassembled prescriptions were predicted utilizing the SwissTargetPrediction database, a total of 1,140 FZP targets, 907 YYP targets, and 923 JDP targets were identified. A total of 646 targets were shared across the three combinations (Figure 1A). Accordingly, we constructed a TCM-component-target network consisting of 1,535 nodes and 17,769 edges (Figure 1B). The red V-shaped nodes in the network represent YFJP. The purple triangle nodes represent YYP, FZP, and JDP, respectively. Circular nodes of orange color signify YYP, FZP, and JDP. Diamond nodes of blue color signify the active ingredients of FZP, diamond nodes of yellow color signify the active ingredients of JDP, diamond nodes of green signify the active ingredients of

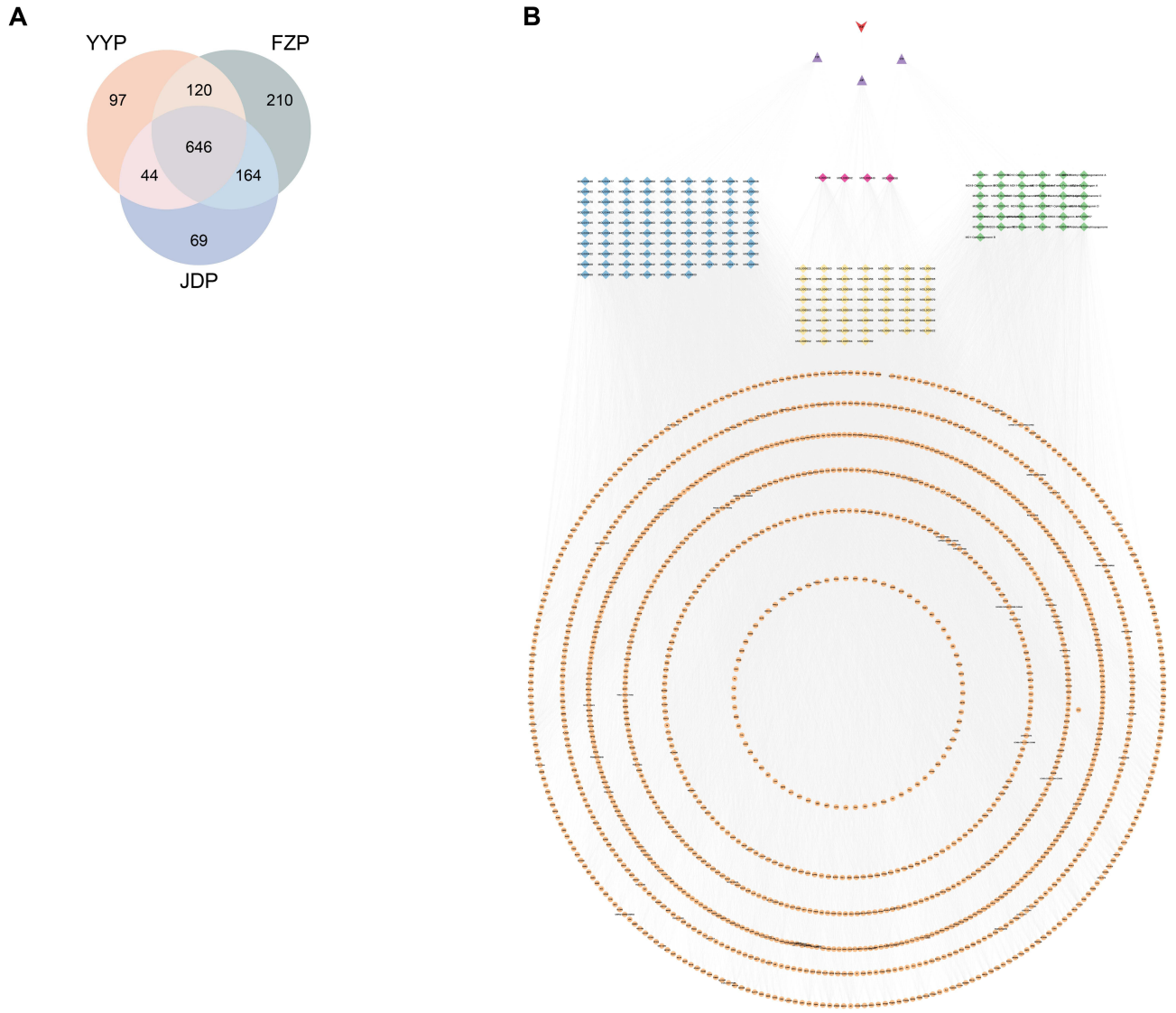

Figure 1 Construction of the TCM-component-target network. **(A)** Venn diagram of the therapeutic targets of the three disassembled prescriptions of YFJP. **(B)** TCM-component-target network.

YYP, and rose-red diamond nodes represent stigmasterol and quercetin, which are common YYP, FZP, and JDP ingredients. Formononetin is a common ingredient in JDP and FZP. Beta-sitosterol is a shared component of YYP and JDP.

Prediction of Therapeutic Targets and Active Components

To screen the hub targets and active ingredients of YFJP, The PPI network was constructed. By intersecting the predicted targets of YFJP with those of HCC, 765 therapeutic targets of YFJP on HCC were identified to construct the PPI network. The PPI network is composed of 765 nodes and 2,833 edges (Figure 2A). The edges in the network represent the interactions between the targets. To delve deeper into the effects of YFJP on HCC therapy, a cluster analysis based on the MCODE and ClusterONE method was conducted on the PPI network, the 165 nodes significantly clustered were used to reversely select the putative active ingredients from the TCM-component-target network, which was utilized for the development of the TCM-component-target-HCC network (Figure 2B). The network comprised 346 nodes and 3,320 edges. The red V-shaped node represents YFJP; the red node of the parallelogram represents HCC; the nodes symbolized by purple triangles denote YYP, FZP, and JDP; the nodes symbolized by orange circular denote the 165 significantly

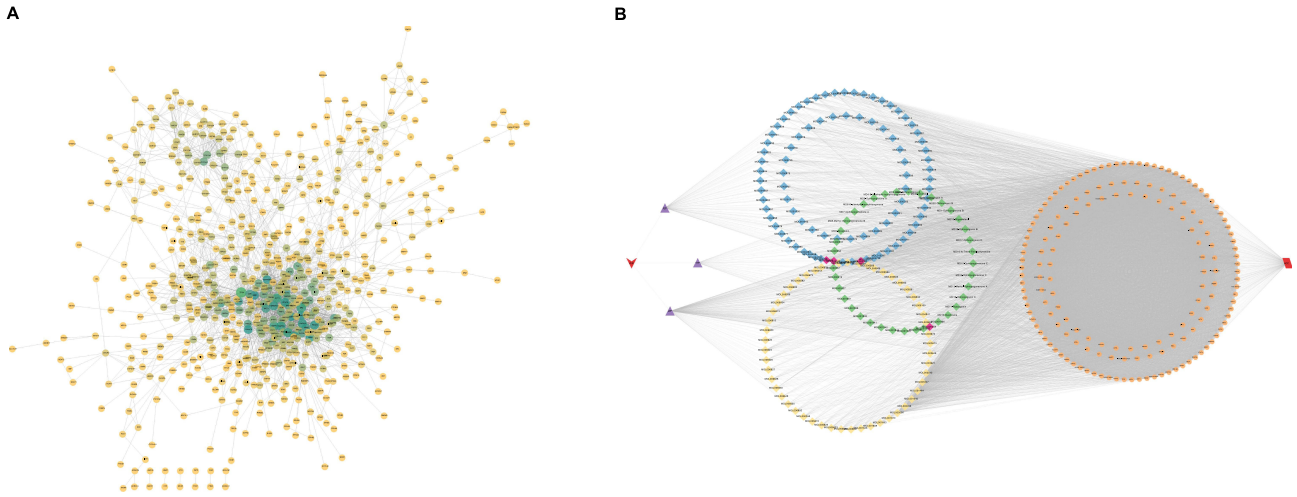

Figure 2 Screening of the hub targets and active ingredients of YFJP for HCC treatment. **(A)** PPI network of YFJP for HCC treatment. **(B)** TCM-component-target-HCC composite network.

clustered nodes; the nodes symbolized by blue diamond denote 84 FZP components; the green diamond nodes represent 37 YYP components; and the nodes symbolized by yellow diamond denote 51 JDP components. The rose-red diamond nodes represent stigmasterol, quercetin, formononetin, and beta-sitosterol, which are common active components among the disassembled prescriptions, as mentioned above. Furthermore, topology analysis of the TCM-component-target-HCC network was performed. Ranked from high to low by Degree (De) value, the top five components and the top 5% of targets were retained for further molecular docking analysis.

Molecular Docking Analysis

To ascertain the binding affinity between targets and components, a molecular docking analysis was conducted. A cohort of 40 protein-ligand complexes exhibited favorable binding affinities, characterized by binding energies below the threshold of −7 kcal/mol (Figure 3A). MAPK3-Saikogenin F (affinity = −9.8 kcal/mol) (Figure 3B), EGFR-saikogenin F (affinity = −9.7 kcal/mol) (Figure 3C), and PIK3CA-Saikogenin F (affinity = −8.9 kcal/mol) (Figure 3D) displayed the strongest binding activity. These three pairs of complexes were subjected to Pymol-based 3D and LigPlot-based 2D visualization to verify their protein-ligand binding abilities. Saikogenin F was found to form hydrogen bonds with MAPK3, EGFR and PIK3CA.

FOXO1 is the Key Transcription Factor Regulated by YFJP in the Treatment of HCC

To further explore the key transcription factors regulated by core targets, we used MAPK3, EGFR, and PIK3CA to construct a transcriptional regulatory network (Figure 4A). The network comprised 145 nodes and 254 edges. The blue triangle nodes denote the three core targets, whereas the green diamond nodes denote transcription factors. Topological analysis of the transcriptional regulatory network revealed that among the transcription factors co-regulated by MAPK3, EGFR, and PIK3CA, FOXO1 had the highest topological coefficient.

To assess the expression levels of FOXO1 in HCC, we compared the relative expression profiles of FOXO1 between tumor tissues and corresponding non-neoplastic liver tissues, leveraging data from The Cancer Genome Atlas (TCGA) project. Compared to non-neoplastic liver tissues, the expression level of FOXO1 is lower in liver cancer tissue, with a statistically significant difference found (P = 6.4e-13) in TCGA database (Figure 4B). According to previous studies, FOXO1 participates in the regulation of tumor prognosis via several mechanisms.[19,20] As the expression level of FOXO1 is known to significantly reduced in HCC, we opted to elucidate the changes in prognosis caused by its low expression. Kaplan-Meier survival analysis was employed to assess the prognostic significance of FOXO1 expression levels on overall survival (OS) (Figure 4C). The median survival times with high and low FOXO1 expression were 49.5 months and 80.4 months, respectively. The Kaplan-Meier estimated 1-, 3-, and 5-year overall survival rates for the high FOXO1

https://doi.org/10.2147/DDDT.S492576

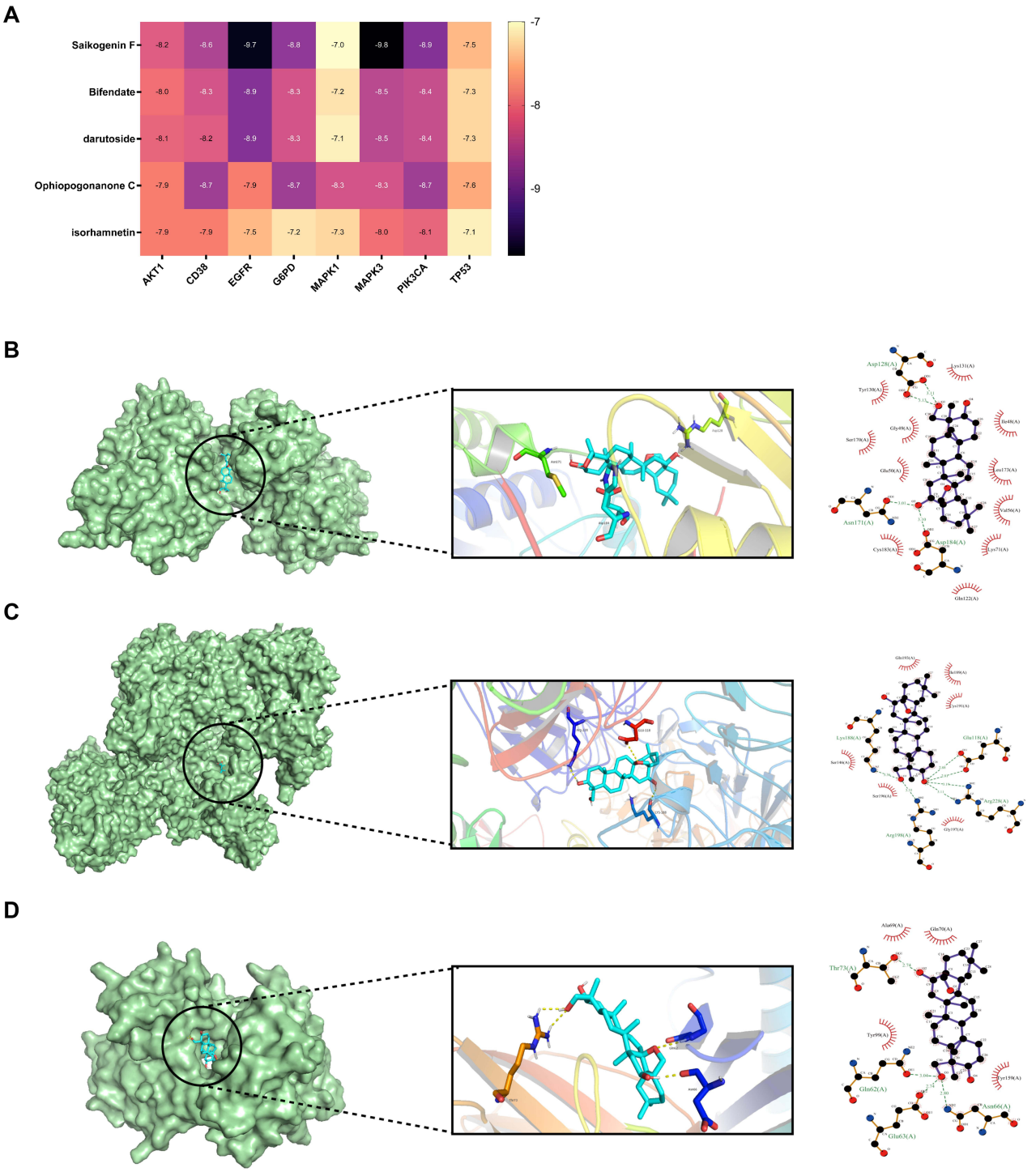

Figure 3 Molecular docking was operated to analyse the binding activity of targets and active ingredients. **(A)** Binding energy of the active ingredient and target. **(B-D)** 3D and 2D visualizations were performed to verify the binding mode of Saikogenin F with MAPK3 **(B)**, EGFR **(C)**, and PIK3CA **(D)**.

expression cohort were 79.2%, 57.0%, and 48.4%, respectively, whereas the overall survival rates for the low FOXO1 expression cohort were 78.9%, 17.7%, and 60.0%, respectively. According to the Kaplan-Meier survival estimates, the cumulative overall survival rates for the cohort with high FOXO1 expression were significantly superior to those of the cohort with low FOXO1 expression. (HR=0.55, 95% CI 0.38–0.80, p=0.006).

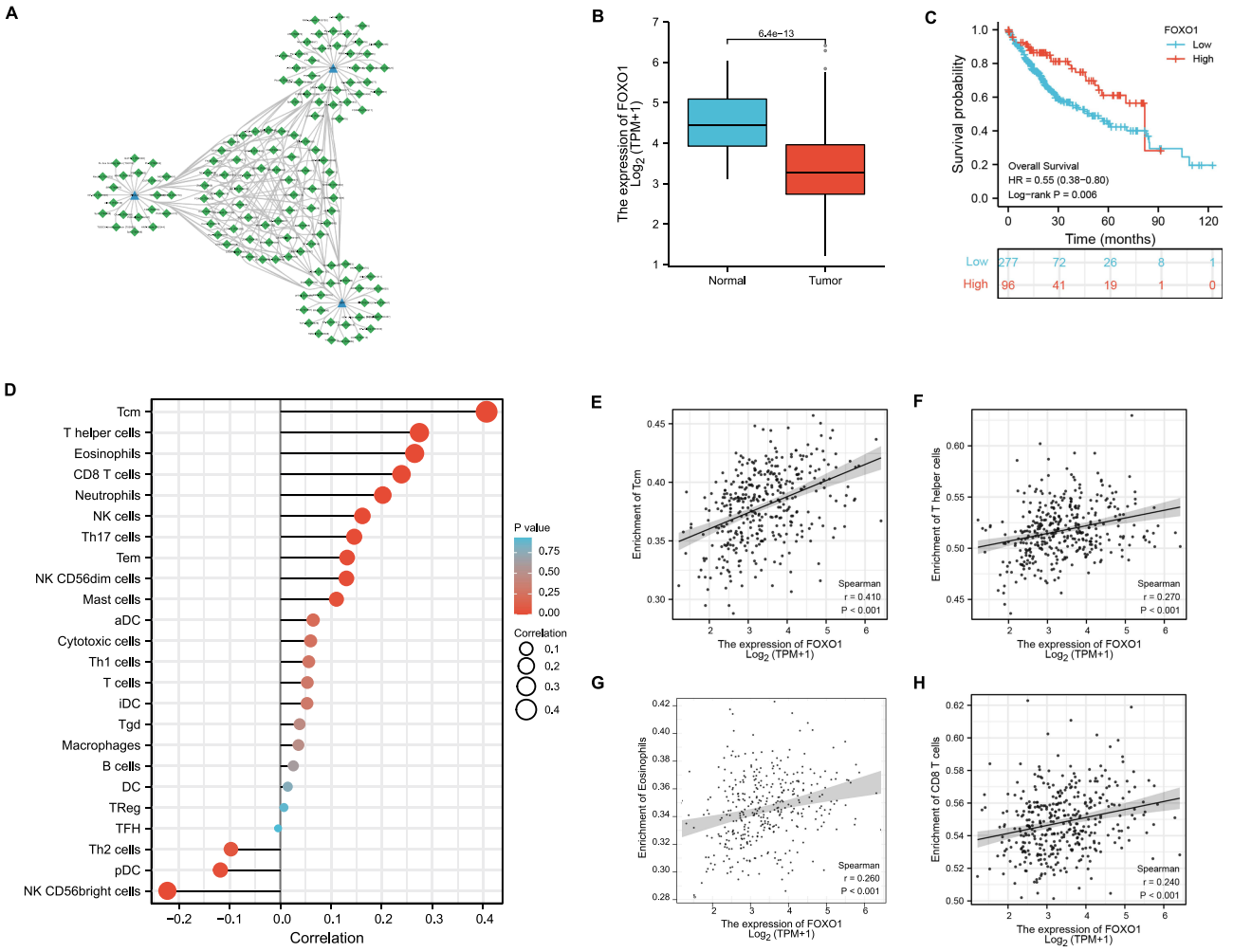

Figure 4 FOXO1 is an independent protective factor for the survival outcome of patients with HCC, and it is a key transcription factor regulated by YFJP. **(A)** Transcriptional regulatory network. **(B)** Based on the analysis of the HCC patient cohort in the TCGA database, the expression level of FOXO1 was significantly reduced in HCC tissues compared with non-tumor liver tissues. **(C)** Survival curves for overall survival of HCC patients with high and low FOXO1 expression. **(D)** Differential expression analysis of 24 tumor infiltrating lymphocytes in the immune microenvironment of HCC. (**E-H**) Correlation analysis of infiltration levels of T_{cm}, $CD8^+$ T Cells, Helper T Cells, and Eosinophils with FOXO1 expression levels. Spearman correlation was used to determine the P value.

Meanwhile, the relationship between FOXO1 and immune cells was analyzed using TCGA database (Figure 4D). Levels of T_{cm}, T helper cells, Eosinophils, $CD8^+$ T cells, Neutrophils, NK cells, and NK $CD56_{dim}$ cells were most strongly correlated with FOXO1 level ($p < 0.05$). Spearman correlation analysis was used (Figure 4E–H). A statistically significant positive correlation was found between T_{CM} ($p < 0.0501$), T helper cells ($p < 0.001$), $CD8^+$ T cells ($p < 0.001$), and Eosinophils ($p < 0.05$) of tumor-infiltrating immune cells. The findings suggest that HCC tissues exhibit significantly reduced FOXO1 expression compared to the adjacent non-tumorous liver tissues. Furthermore, FOXO1 may serve as an independent prognostic biomarker in HCC patients, and its expression is positively associated with the level of T cell infiltration.

KEGG and GO Analyses

KEGG and GO analyses were performed on the nodes with De greater than the mean in the PPI network. The results of the enrichment analysis were presented with signaling pathways and biological functions listed in order of p-value from smallest to largest (Figure 5). The key signaling pathways of YFJP in treating HCC include the FoxO signalling pathway, the Chemokine signaling pathway, Autophagy, as well as Cellular senescence (Figure 5A). GO enrichment analysis

https://doi.org/10.2147/DDDT.S492576

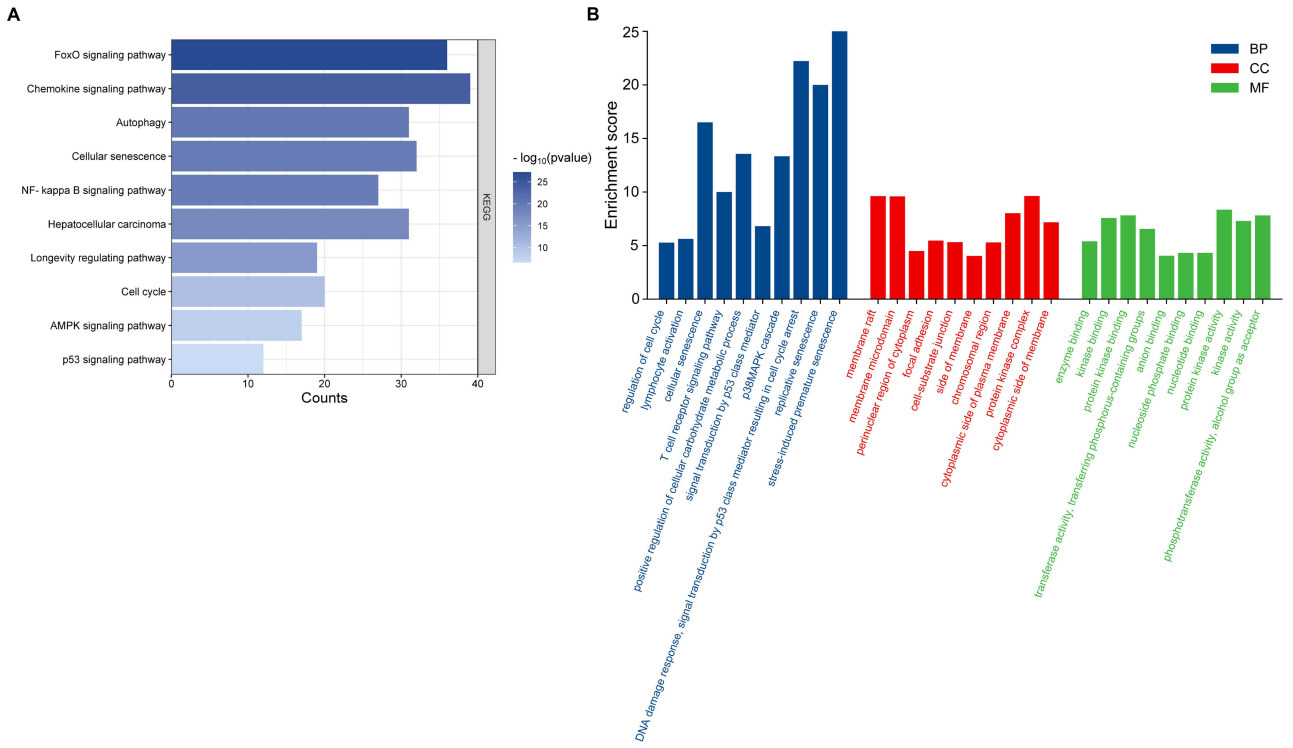

Figure 5 (A) KEGG pathway enrichment. **(B)** GO functional enrichment.

revealed stress-induced premature senescence, signal transduction by p53 class mediators, resulting in cell cycle arrest, replicative senescence, DNA damage response, cellular senescence and other biological processes (Figure 5B).

YFJP Regulates T Cell Proportions in Peripheral Blood of Patients with HCC

Flow cytometry was employed to determine the effects of YFJP on various T cell subsets in the peripheral blood of patients with HCC. The proportions of $CD3^+$ T cells, $CD4^+$ T cells, $CD8^+$ T cells, and Tregs were compared among age-matched patients with HCC who received conservative treatment alone or combined with YFJP or an immune checkpoint inhibitor (ICI) (Figure 6A). Compared to conservative treatment, treatment with YFJP significantly increased the proportion of $CD3^+$ T cells in the peripheral blood of patients with HCC ($p < 0.01$), decreased the proportion of Tregs ($p < 0.0001$), and increased $CD8^+$ T cell proportion ($p < 0.05$). Compared with ICI treatment, treatment with YFJP significantly increased the proportion of $CD3^+$ T cells ($p < 0.05$), reduced the proportion of Tregs ($p < 0.01$), and increased $CD8^+$ T cell proportion ($p < 0.05$).

The crucial role of cytotoxic T lymphocytes (CTLs) in mediating anti-tumor immune reactions is well-established, to further investigate the regulatory influence of YFJP on CD8+ T cells in the HCC immune microenvironment, we compared the proportions of naïve $CD8^+$T cells (T_n), central memory $CD8^+$ T cells (T_{cm}), effector memory $CD8^+$ T cells (T_{em}), and terminally differentiated effector $CD8^+$ T cells (T_{emra}) among the three groups (Figure 6B). Compared to conservative treatment and ICI treatment, treatment with YFJP significantly increased the proportion of T_{em} and decreased the proportion of T_{emra} ($p < 0.05$).

YFJP Reduces Senescent $CD8^+$ T Cell Proportion in Tumor-Bearing Mice

To identify known components of YFJP, we performed HPLC detection, the two main peaks of YFJP as matrine and oxymatrine were identified in the serum of H22 tumor-bearing mice (Supplementary Figure 1B) compared with the standard control (Supplementary Figure 1A). The results provide a theoretical basis for subsequent research.

Using samples of patients with HCC, we found that the T cell subset regulated by YFJP was $CD8^+$T cells. Based on KEGG and Go analysis, the main signaling pathway regulated by YFJP was cell senescence signaling pathway. In order to verify the

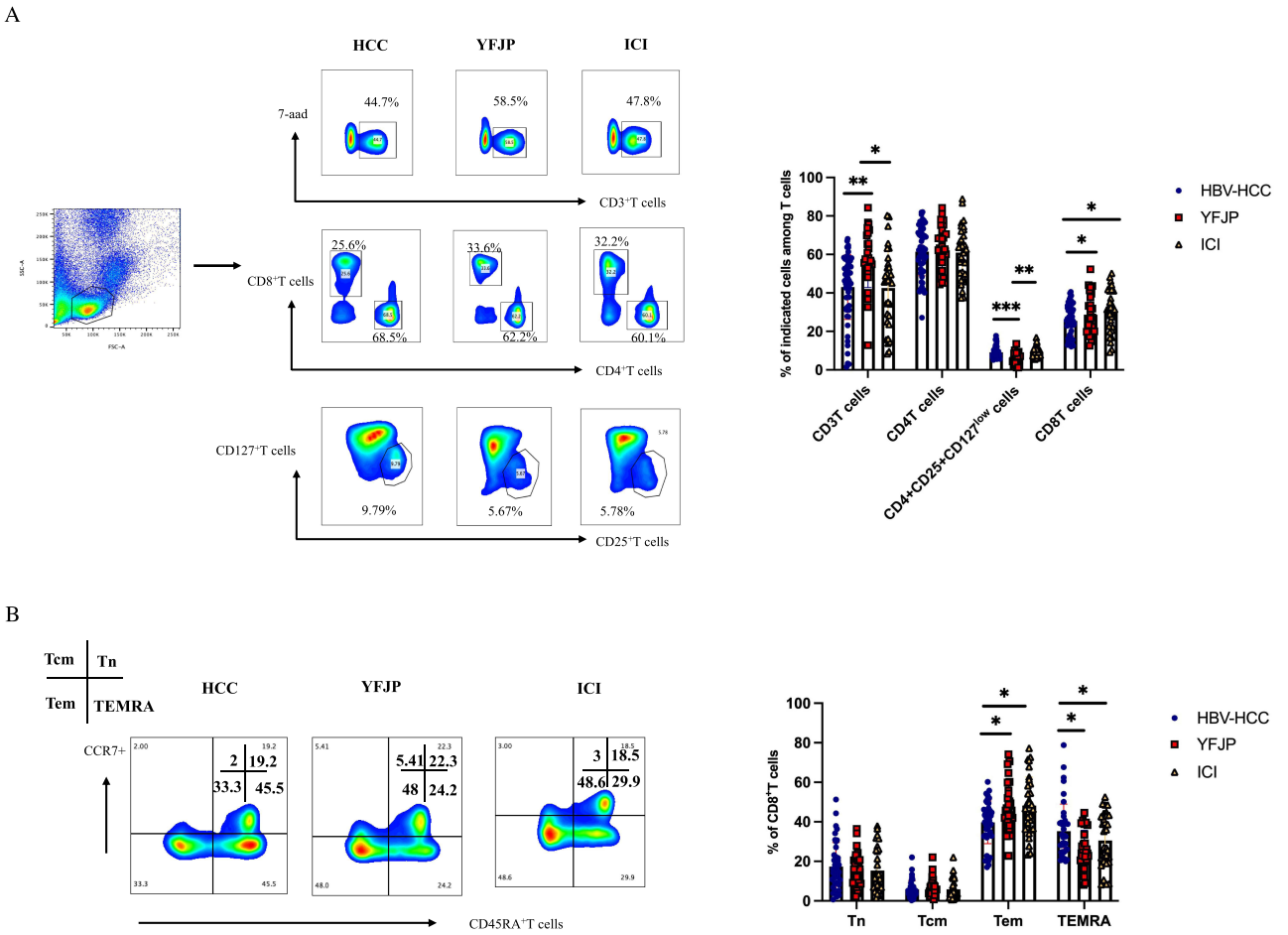

Figure 6 Flow cytometry measured T cell subset proportions of HCC patients treated with YFJP or ICI. **(A)** YFJP or ICI increased the proportion of $CD3^+$ T cells and $CD8^+$ T cells and decreased the number of Tregs in the peripheral blood of patients with HCC. **(B)** YFJP or ICI increased the proportion of T_{em} and decreased the proportion of T_{emra} in the peripheral blood of patients with HCC. Patients with HCC were administered with conventional therapy (n=56), YFJP (n=27), or YFJP plus ICI (n=32). Data are shown as mean±SEM. * $p < 0.05$, ** $p < 0.01$, *** $p < 0.001$.

effect of YFJP on $CD8^+$T cell senescence in the immune microenvironment of HCC. The expression level of SA-β-Gal in $CD8^+$ T cells of H22 tumor-bearing mice was detected (Figure 7A–C). The results demonstrated that the expression of SA-β-Gal in $CD8^+$ T cells from the peripheral blood and spleen of the model group was significantly higher than that in the control group ($p < 0.05$) (Figure 7A–B). The expression of SA-β-Gal on CD8+T cells in peripheral blood, spleen and tumor tissues was significantly lower than in the YFJPM group compared with the model group ($p < 0.01$) (Figure 7A–C).

YFJP Increases FoxO1 Expression in $CD8^+$ T Cells in Tumor-Bearing Mice

To investigate the regulatory impact of YFJP on the expression of the FoxO1 signaling pathway in H22 tumor-bearing mice, Western blot analysis was employed to evaluate the expression of FoxO1 in $CD8^+$ T cells within tumor tissues (Figure 7D). The findings suggested that, in comparison with the model group, the protein expression of FoxO1 markedly increased in the YFJPH group ($p < 0.05$), and even more so in the YFJPM group ($p < 0.001$). Indicating that YFJP significantly increased the expression ratio of FoxO1 in tumor tissues. Flow cytometry was employed to measure the expression level of FoxO1 in splenic $CD8^+$ T cells of H22 tumor-bearing mice (Figure 7E). The results illustrated that the expression level of FoxO1 in splenic $CD8^+$ T cells was significantly decreased in the model group in contrast to the control group ($p < 0.05$). The expression of FoxO1 in $CD8^+$ T cells was significantly higher in the YFJPM group compared to the model group ($p < 0.05$). The above results were further corroborated by multi-color immunofluorescence staining (Figure 7F–I). Compared with the model group, YFJPM significantly increased the infiltration of $CD8^+$ T cells in tumor tissues (Figure 7G). Both YFJPM and YFJPL significantly reduced the level of SA-β-Gal^+CD8^+ T cells ($p < 0.01$) (Figure 7H). For $FoxO1^+CD8^+$ T cells, intervention with YFJP at high, medium and low doses

https://doi.org/10.2147/DDDT.S492576

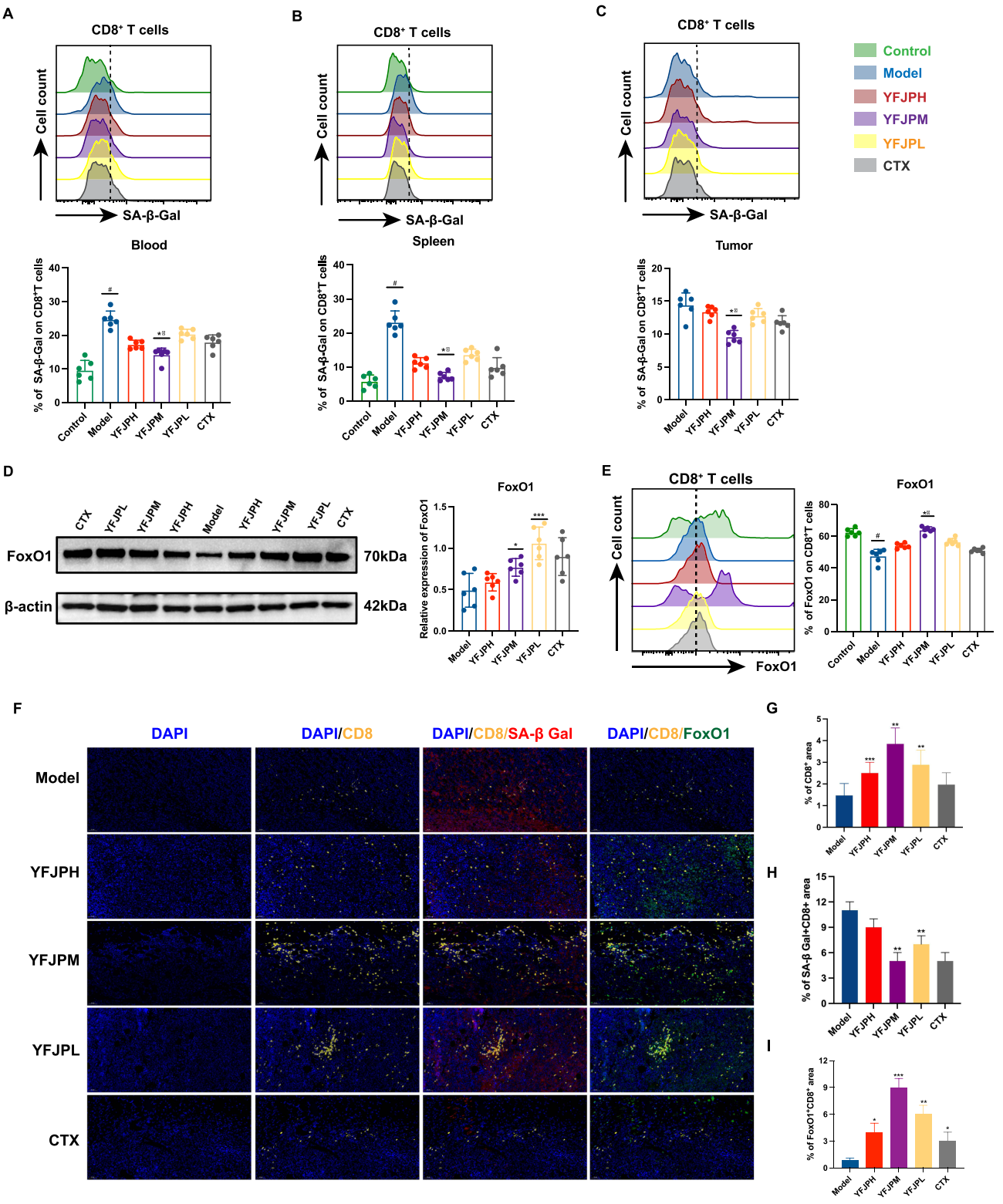

Figure 7 YFJP mediated reduction of senescent CD8$^+$ T cells and upregulation of FoxO1 in tumor-bearing mice. **(A-C)** After H22 tumor-bearing mice received treatment with high, medium, and low doses of YFJP, the expression of SA-β-Gal in CD8$^+$ T cells was assessed in peripheral blood, spleen, and tumor tissues. **(D)** Western blot analysis was employed to assess the expression levels of FoxO1 in tumor tissues of H22 tumor-bearing mice. **(E)** Flow cytometry was utilized to detect the expression of FoxO1 in splenic CD8$^+$ T cells from H22 tumor-bearing mice. **(F)** Multi-color immunofluorescence staining was used to evaluate the immune infiltration status of CD8$^+$ T cells **(G)**, the expression of SA-β-Gal$^+$CD8$^+$ T cells **(H)**, and the expression of FoxO1$^+$CD8$^+$ T cells **(I)** in tumor tissues of H22 tumor-bearing mice. Data are expressed as mean ± SD, with n = 6 mice per group. # $p < 0.05$ vs the Control group, * $p < 0.05$ vs the Model group, ** $p < 0.01$, *** $p < 0.001$, # $p < 0.05$ vs the Control group; Δ $p < 0.05$ vs the CTX group.

https://doi.org/10.2147/DDDT.S492576

or with CTX could increase the expression of FoxO1 on $CD8^+$ T cells, especially at the YFJP medium dose ($p < 0.001$) (Figure 7I). These results indicate that YFJP can reduce senescent $CD8^+$ T cells in H22 tumor-bearing mice and promote FoxO1 expression in $CD8^+$ T cells, with the most significant effect in the middle dose.

FoxO1 is the Target of YFJP in Improving $CD8^+$ T Cell Senescence

To further explore whether FoxO1 is the key molecular target of YFJP in regulating $CD8^+$ T cell senescence, primary $CD8^+$ T cells were sorted cocultured with tumor cell line (Figure 8). After intervention with YFJP and/or FoxO1 inhibitor, $CD8^+$ T cells in the co-culture system were detected with flow cytometry. The results showed that compared with $CD8^+$ T cells cultured alone, the expression levels of SA-β-Gal ($p < 0.05$), p53 ($p < 0.01$), p21 ($p < 0.05$) and p16 ($p < 0.001$) in $CD8^+$ T cells were significantly increased in co-culture group. Compared with co-culture group, YFJP intervention significantly inhibited the expression of SA-β-Gal ($p< 0.01$), p53 ($p< 0.01$), p21 ($p< 0.05$) and p16 ($p< 0.001$) in $CD8^+$ T cells. However, the effect was abolished after pretreating $CD8^+$ T cells with AS1842856, a FoxO1 inhibitor. AS1842856 inhibited FoxO1-mediated trans-activation by directly binding to activated FoxO1,[21] we pretreated primary $CD8^+$ T cells with AS1842856 for 12 hours before coculturing with H22 cell line in the presence of YFJP-containing serum, the inhibitory effects of YFJP on SA-β-Gal and p53 could be rescued ($p < 0.05$). The results showed that YFJP containing serum could improve the senescence of $CD8^+$T cells in the co-culture system, and intervention of the co-culture system with YFJP containing serum after blocking FoxO1 could restore the improvement effect of YFJP containing serum on $CD8^+$T cell senescence. In summary, FoxO1 is a key target through which YFJP improves the senescence of $CD8^+$ T cells in the HCC immune microenvironment.

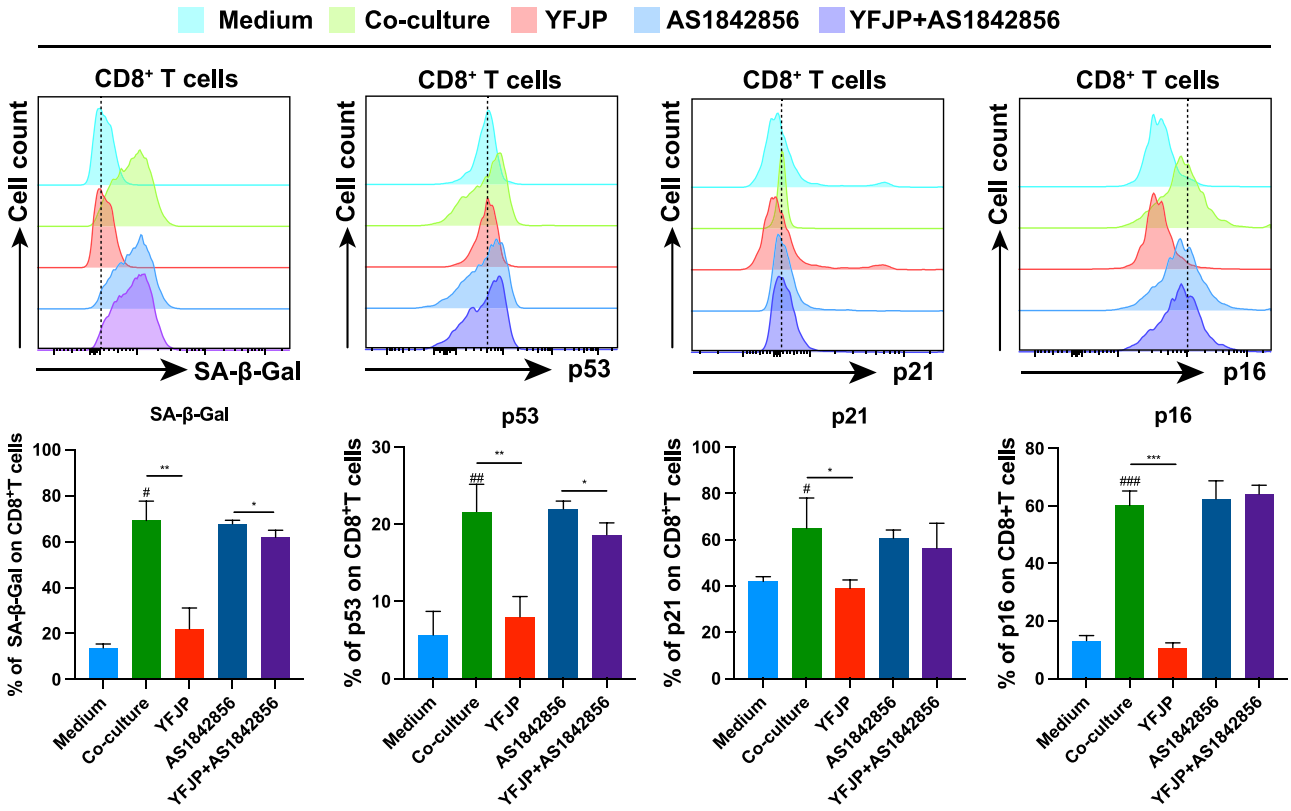

Figure 8 YFJP-containing serum inhibited $CD8^+$ T cell senescence in the co-culture system. The medium group: primary $CD8^+$ T cells were cultured with medium alone; The co-culture group: Primary $CD8^+$ T cells were co-cultured with H22 cell line in the presence of control serum at a 1:1 ratio; The YFJP group: primary $CD8^+$ T cells and H22 cell line were co-cultured at a ratio of 1:1 in the presence of YFJP-containing serum; The AS1842856 group: primary $CD8^+$ T cells were pretreated with FoxO1 inhibitor for 12 hours and then co-cultured with H22 cell line at a ratio of 1:1 in the presence of control serum; The YFJP+AS1842856 group: primary $CD8^+$ T cells were pretreated with FoxO1 inhibitor for 12 hours and then co-cultured with H22 cell line at a ratio in the presence of YFJP drug-containing serum. Data are presented as mean ± standard deviation (SD) from six independent experiments, each repeat was performed as a separate, independent experiment. # $p < 0.05$ vs the Medium group; ## $p < 0.01$ vs the Medium group, ### $p < 0.001$ vs the Medium group. * $p < 0.05$ vs the Co-culture group, ** $p < 0.01$ vs the Co-culture group, *** $p < 0.001$ vs the Co-culture group.

https://doi.org/10.2147/DDDT.S492576

Discussion

HCC is a major health burden worldwide owing to its high morbidity and mortality rates. TCM exhibits multi-target and multi-pathway synergistic actions in the treatment of complex diseases. Accordingly, TCM can attenuate toxicity and exhibit enhanced efficacy in the systemic treatment of HCC. In this study, the molecular targets and active components of YFJP in treating HCC were explored through multi-target network construction, molecular docking, bioinformatics analysis, clinical sample detection, as well as in vivo and in vitro experimental verification.

Through the construction of herb-component-target network, active ingredients of YFJP for HCC treatment were obtained. Saikogenin F is a triterpenoid compound widely present in nature. Several studies have shown that Saikogenin F exhibits varying anti-inflammatory effects and can participate in immune regulation by affecting the activity of immune cells and the production of cytokines.[22–24]

The FoxO subclass comprises four members: FoxO1, FoxO3, FoxO4, and FoxO6. However, only FoxO1 is highly expressed in B cells, T cells. According to previous studies, FoxO1 plays an important role in combating cellular senescence and promoting the prolongation of cell lifespan by participating in several key biological processes, such as anti-oxidative stress, DNA repair, cell cycle regulation, cell autophagy, and metabolic regulation.[25,26] In KEGG pathway enrichment analysis, we found that the potential targets of YFJP for HCC treatment were significantly enriched in FoxO signaling pathway. Furthermore, FoxO1 was identified to be the core transcription factor in YFJP treatment of HCC by transcriptional regulatory network construction and topological analysis. Based on TCGA database, the expression of FOXO1 in HCC tissues and the prognosis of patients were analyzed. The results revealed that FOXO1 expression was significantly increased in tumor tissues of patients with HCC compared with adjacent tissues, FOXO1 was a protective factor for overall survival. FOXO1 was positively correlated with the infiltration level of a variety of immune cells, and 50% of the top 20 immune cells belonged to T cell subsets. By prospectively collecting PBMCs from patients with HCC, we analyzed the distribution of T cell subpopulations. Our study shows that YFJP administration significantly bolstered the proportion of $CD8^+$ T cells, expanded their memory subset, and diminished the terminally differentiated $CD8^+$ T cells. This discovery is in concordance with the results from preceding animal model studies.[4] In tumor-bearing mice, we observed that YFJP treatment could significantly increase the expression of FoxO1 on $CD8^+$ T cells in the immune microenvironment of HCC.

Immunosenescence is an innate and adaptive immune dysfunction caused by the structural destruction and remodeling of tissues and organs during aging.[27] Cellular senescence is a stable state of cell cycle arrest, and the accumulation of senescent cells has been shown to accelerate the onset of a variety of diseases in humans, mice, and some other species.[28] $CD8^+$ T cell senescence is one of the most important manifestations of immune senescence. According to several studies, the number of senescent $CD8^+$T cells increases in TILs.[29] In the immune microenvironment of HCC, tumor-derived inflammatory factors can promote the progress of $CD8^+$ T cell senescence. Glucose competition exists between various immunosuppressive cells and T cells in the immune microenvironment of HCC, which induces senescence of responding T cells. In addition, the accumulation of metabolic end products and the continuous repetitive stimulation of tumor antigens also contribute to T cell senescence.[30] An increase in the number and size of lysosomes associated with Senescence-Associated β-Galactosidase (SA-β-Gal) activity is the most typical feature of senescent cells. The expression of SA-β-Gal is considered the "gold standard" of senescent cells.[13] In addition, cell cycle arrest is another typical features of senescent cells, the activation of p53, p16 and p21 occurs in cell cycle arrest, and cyclins are also biomarkers of cellular senescence. Senescent T cells exhibit reduced effector function, proliferation inhibition, as well as senescence-associated secretory phenotype (SASP).[31] SASP refers to the secretion of a variety of immunosuppressive cytokines including IL-6, IL-10, TGF-β, which aggravate the formation of liver cancer immunosuppressive microenvironment. Therefore, T cell senescence is a potential target for HCC immunotherapy.

Through KEGG and GO analysis, we identified that YFJP contributes to HCC treatment through regulating cellular senescence signaling pathway and cell senescence-related biological processes. Using a tumor bearing mice model, our study validated that YFJP treatment reduces the percentage of SA-β-Gal^+CD8^+ T cells in HCC immune microenvironment. These results indicated that YFJP inhibited $CD8^+$T cell senescence. By co-culturing primary $CD8^+$ T cells with an HCC cell line and treating them with YFJP and FoxO1 inhibitor, we confirmed that FoxO1 was the core target of YFJP in improving $CD8^+$ T cell senescence.

Conclusion

In conclusion, the mechanism of YFJP in the treatment of HCC involves multiple targets and signaling pathways. This study confirmed that YFJP can improve $CD8^+$ T cell senescence in the HCC immune microenvironment, FoxO1 is the key molecular target of YFJP in improving $CD8^+$ T cell senescence. This study preliminarily clarified the mechanism of YFJP in regulating immunosenescence of HCC, and provided an in-depth insight into the mechanism of action of YFJP in the treatment of HCC and a theoretical basis for the use of TCM to treat HCC through multiple pathways and targets.

Data Sharing Statement

All data generated or analyzed during this study are included in this published article.

Ethics Statement

Experiments involving human samples has been approved by the Ethics Committee of Ditan Hospital, affiliated with Capital Medical University, Beijing, and has obtained informed consent from the participants, The ethics NO.DTEC-KY2023-014-02.

Animal experiments were approved by the Animal Ethics Committee of the Animal Care and Use Committee of Beijing University of Chinese Medicine and strictly performed according to the Guide for the Care and Use of Laboratory Animals published by the US National Institutes of Health (Experimental Animal Ethics Certificate No. BUCM-4-2021062301-2067).

Author Contributions

All authors made a significant contribution to the work reported, whether that is in the conception, study design, execution, acquisition of data, analysis and interpretation, or in all these areas; took part in drafting, revising or critically reviewing the article; gave final approval of the version to be published; have agreed on the journal to which the article has been submitted; and agree to be accountable for all aspects of the work.

Funding

This work was supported by the National Science Foundation of China (No.82274479 and 82104781), Beijing Research Ward Excellence Program, BRWEP (NO.BRWEP2024W10217010), High-level Public Health Technical Personnel Construction Project (Subject leaders-02-16), Key Medical Professional Development Program (No.ZYLX202127), Beijing Hospitals Authority Youth Programme (QML20231801), Capital Medical University Research and Translational Laboratory for Traditional Chinese Medicine in the Prevention and Treatment of Infectious Severe Hepatitis, National key research and development program (2024YFC3044700), Research and development of Yangyin Fuzheng Jiedu Prescription for Liver Cancer Medical institutions (DTTP-202301), Beijing Municipal Administration of Traditional Chinese Medicine's New Era 125 Talent Project-Leading Talents.

Disclosure

The authors declare that they have no known competing financial interests or personal relationships that could have appeared to influence the work reported in this paper.

References

1. Sung H, Ferlay J, Siegel RL, et al. Global cancer statistics 2020: globocan estimates of Incidence and mortality worldwide for 36 cancers in 185 countries. *CA Cancer J Clin*. 2021;71(3):209–249. doi:10.3322/caac.21660
2. Chan LL, Chan SL. Drug development for hepatocellular carcinoma. *Lancet Oncol*. 2023;24(12):1292–1294. doi:10.1016/S1470-2045(23)00523-5
3. Yang X, Yang C, Zhang S, et al. Precision treatment in advanced hepatocellular carcinoma. *Cancer Cell*. 2024;42(2):180–197. doi:10.1016/j.ccell.2024.01.007
4. Yan F, Wang X, Xie Y, et al. Yangyin fuzheng jiedu prescription exerts anti-tumor immunity in hepatocellular carcinoma by alleviating exhausted T cells. *Phytomedicine*. 2021;91:153722. doi:10.1016/j.phymed.2021.153722
5. Liu X, Li M, Wang X, et al. Effects of adjuvant traditional Chinese medicine therapy on long-term survival in patients with hepatocellular carcinoma. *Phytomedicine*. 2019;62:152930. doi:10.1016/j.phymed.2019.152930

6. Yan F, Feng M, Wang X, et al. Molecular targets of yangyin fuzheng jiedu prescription in the treatment of hepatocellular carcinoma based on network pharmacology analysis. *Cancer Cell Int*. 2020;20(1):540. doi:10.1186/s12935-020-01596-y
7. Xie Y, Yan F, Wang X, et al. Mechanisms and network pharmacological analysis of yangyin fuzheng jiedu prescription in the treatment of hepatocellular carcinoma. *Cancer Med*. 2023;12(3):3237–3259. doi:10.1002/cam4.5064
8. Tf G, Cw L, Kf SO. Targeted and immune-based therapies for hepatocellular carcinoma. *Gastroenterology*. 2019;156(2). doi:10.1053/j.gastro.2018.09.051
9. Barkley D, Moncada R, Pour M, et al. Cancer cell states recur across tumor types and form specific interactions with the tumor microenvironment. *Nat Genet*. 2022;54(8):1192–1201. doi:10.1038/s41588-022-01141-9
10. Dai D, Pei Y, Zhu B, et al. Chemoradiotherapy-induced ACKR2+ tumor cells drive CD8+ T cell senescence and cervical cancer recurrence. *Cell Rep Med*. 2024;5(5):101550. doi:10.1016/j.xcrm.2024.101550
11. Liu Z, Liang Q, Ren Y, et al. Immunosenescence: molecular mechanisms and diseases. *Signal Transduct Target Ther*. 2023;8(1):200. doi:10.1038/s41392-023-01451-2
12. Wang L, Lankhorst L, Bernards R. Exploiting senescence for the treatment of cancer. *Nat Rev Cancer*. 2022;22(6):340–355. doi:10.1038/s41568-022-00450-9
13. Lee BY, Han JA, Im JS, et al. Senescence-associated beta-galactosidase is lysosomal beta-galactosidase. *Aging Cell*. 2006;5(2):187–195. doi:10.1111/j.1474-9726.2006.00199.x
14. Liu X, Hoft DF, Peng G. Senescent T cells within suppressive tumor microenvironments: emerging target for tumor immunotherapy. *J Clin Investig*. 2020;130(3):1073–1083. doi:10.1172/JCI133679
15. Ru J, Li P, Wang J, et al. TCMSP: a database of systems pharmacology for drug discovery from herbal medicines. *J Cheminform*. 2014;6:13. doi:10.1186/1758-2946-6-13
16. Daina A, Michielin O, Zoete V. SwissTargetPrediction: updated data and new features for efficient prediction of protein targets of small molecules. *Nucleic Acids Res*. 2019;47(W1):W357–W364. doi:10.1093/nar/gkz382
17. Szklarczyk D, Kirsch R, Koutrouli M, et al. The STRING database in 2023: protein-protein association networks and functional enrichment analyses for any sequenced genome of interest. *Nucleic Acids Res*. 2023;51:D638–D646. doi:10.1093/nar/gkac1000
18. Nassar LR, Barber GP, Benet-Pagès A, et al. The UCSC genome browser database: 2023 update. *Nucleic Acids Res*. 2023;51:D1188–D1195. doi:10.1093/nar/gkac1072
19. Liu X, Li M, Wang X, et al. PD-1+ TIGIT+ CD8+ T cells are associated with pathogenesis and progression of patients with hepatitis B virus-related hepatocellular carcinoma. *Cancer Immunol Immunother*. 2019;68(12):2041–2054. doi:10.1007/s00262-019-02426-5
20. Cichocki F, Zhang B, Wu CY, et al. Nicotinamide enhances natural killer cell function and yields remissions in patients with non-Hodgkin lymphoma. *Sci Transl Med*. 2023;15(705):eade3341. doi:10.1126/scitranslmed.ade3341
21. Zhang M, Sui W, Xing Y, et al. Angiotensin IV attenuates diabetic cardiomyopathy via suppressing FoxO1-induced excessive autophagy, apoptosis and fibrosis. *Theranostics*. 2021;11(18):8624–8639. doi:10.7150/thno.48561
22. Chen C, Gong W, Tian J, et al. Radix paeoniae alba attenuates radix bupleuri-induced hepatotoxicity by modulating gut microbiota to alleviate the inhibition of saikosaponins on glutathione synthetase. *J Pharm Anal*. 2023;13(6):640–659. doi:10.1016/j.jpha.2023.04.016
23. Lee JE, Song BK, Kim JH, Siddiqi MZ, Im W-T. Production of prosaikogenin f, prosaikogenin g, by the recombinant enzymatic hydrolysis of saikosaponin and their anti-cancer effect. *Molecules*. 2022;27(10):3255. doi:10.3390/molecules27103255
24. Chen C, Yin Q, Tian J, et al. Studies on the changes of pharmacokinetics behaviors of phytochemicals and the influence on endogenous metabolites after the combination of radix bupleuri and radix paeoniae alba based on multi-component pharmacokinetics and metabolomics. *Front Pharmacol*. 2021;12:630970. doi:10.3389/fphar.2021.630970
25. Liu F, Lu Y, Wang X, et al. Identification of FOXO1 as a geroprotector in human synovium through single-nucleus transcriptomic profiling. *Protein Cell*. 2023:pwad060. doi:10.1093/procel/pwad060
26. Delpoux A, Lai CY, Hedrick SM, Doedens AL. FOXO1 opposition of CD8 $^{+}$ T cell effector programming confers early memory properties and phenotypic diversity. *Proc Natl Acad Sci USA*. 2017;114(42). doi:10.1073/pnas.1618916114
27. Santoro A, Bientinesi E, Monti D. Immunosenescence and inflammaging in the aging process: age-related diseases or longevity? *Ageing Res Rev*. 2021;71:101422. doi:10.1016/j.arr.2021.101422
28. González-Gualda E, Baker AG, Fruk L, Muñoz-Espín D. A guide to assessing cellular senescence in vitro and in vivo. *FEBS J*. 2021;288(1):56–80. doi:10.1111/febs.15570
29. Liu X, Si F, Bagley D, et al. Blockades of effector T cell senescence and exhaustion synergistically enhance antitumor immunity and immunotherapy. *J Immunother Cancer*. 2022;10(10):e005020. doi:10.1136/jitc-2022-005020
30. Tedeschi V, Paldino G, Kunkl M, et al. CD8+ T cell senescence: lights and shadows in viral infections, autoimmune disorders and cancer. *Int J mol Sci*. 2022;23(6):3374. doi:10.3390/ijms23063374
31. Goronzy JJ, Weyand CM. Mechanisms underlying T cell ageing. *Nat Rev Immunol*. 2019;19(9):573–583. doi:10.1038/s41577-019-0180-1